Beryllium δ doping of GaAs grown by molecular beam epitaxy

E. F. Schubert, J. M. Kuo, R. F. Kopf, H. S. Luftman, L. C. Hopkins, and N. J. Sauer[a)]
AT&T Bell Laboratories, Murray Hill, New Jersey 07974

(Received 19 July 1989; accepted for publication 17 October 1989)

Spatial localization of Be in δ-doped GaAs within few lattice constants (< 20 Å) is achieved at low growth temperatures for concentrations $N_{\rm Be}^{\rm 2D} < 10^{14}$ cm^{-2} as indicated by capacitance-voltage profiles and secondary ion mass spectroscopy. At elevated growth temperatures and at higher Be concentrations, significant spreading of the dopants occurs and is explained by (i) Fermi-level pinning-induced segregation, (ii) repulsive Coulomb interaction of dopants, and (iii) diffusion. The highest Be concentration achieved at low growth temperatures exceeds 2×10^{20} cm^{-3} and is limited by repulsive dopant interaction. It is shown that the repulsive Coulomb interaction results in a correlated, nonrandom dopant distribution. The diffusion coefficient of Be in GaAs is determined and is found to be much lower than previously reported.

I. INTRODUCTION

The reduction of the spatial dimensions in semiconductor structures and devices requires that dopant distributions are scaled down as well. It is thus desirable to achieve *narrower* distributions and simultaneously *higher* doping concentrations. If the doping distribution becomes narrower than the spatial extent of the electron wave function, then the doping profile can be described by Dirac's δ function. Such δ-functionlike doping distributions are achieved in semiconductors, if dopants are confined to one or few atomic monolayers, i.e., if the width of the dopant distribution is comparable to the lattice constant.

Experimentally, δ-functionlike doping profiles are achieved by growth interruption during epitaxial growth by molecular beam epitaxy (MBE). A schematic sketch of the components within the ultrahigh vacuum chamber of the MBE system are shown in Fig. 1(a). The constituent elements of the semiconductor (e.g., Ga and As) and its dopants (e.g., Be) are evaporated from resistively heated Knudsen cells, whose temperature is monitored by thermocouples. The effusion cells are equipped with shutters to initiate or terminate growth within a fraction of a second. Epitaxial growth is induced on the heated substrate, which is rotated to achieve improved uniformity. In order to achieve δ-functionlike doping profiles in GaAs, the epitaxial growth is suspended by closing the Ga effusion cell without interrupting the As_4 flux to maintain an As-stabilized surface. Subsequently, the dopant effusion cell is opened; the dopant is evaporated on the nongrowing GaAs surface. After evaporation of dopants regular crystal growth is resumed. Under "ideal" conditions; that is, in the absence of diffusion or segregation, the dopants are confined to a single atomic plane in the semiconductor lattice, as shown in Fig. 1(b).

Historically, it was realized about one decade ago, that dopants are incorporated on nongrowing crystal surfaces: Bass[1] found that Si strongly adsorbs to the GaAs surface before epitaxial growth was initiated. He demonstrated that sharp doping spikes can be produced by this technique. Wood *et al.*[2] pointed out the versatility of the technique and the possibility to generate arbitrary doping profiles, if dopants can be confined to a single atomic plane. Subsequently, the δ function was used to represent the doping profile[3] and such doping distributions were employed to improve field-effect transistors. However, only recently it was demonstrated that Si dopants can, in fact, be spatially localized on the length scale of the lattice constant in GaAs. Schubert *et al.*[4] concluded that Si dopants diffuse no more than two lattice constants during subsequent crystal growth. Thus, even though dopants may not be confined to a single atomic plane, the doping profiles are still δ functionlike, if the dopant distribution is much narrower than the spatial extent of the carrier ground-state wave function.

In this article we investigate Be δ doping of GaAs. Our study focuses on the (i) spatial localization of Be in GaAs as measured by secondary ion mass spectroscopy (SIMS) and capacitance-voltage (*C-V*) profiles, (ii) the diffusion of Be in GaAs including the determination of the temperature-dependent diffusion coefficient, (iii) the segregation of Be due to Fermi-level pinning, and (iv) impurity correlation effects at high-doping concentrations.

II. EXPERIMENT

The Be-doped GaAs epitaxial layers are grown in a Varian Gen II molecular beam epitaxy (MBE) system on semi-insulating and Zn-doped (001) GaAs substrates at the four growth temperatures 400, 500, 580, and 660 °C. The GaAs growth rate is 0.9 μm/h. During growth interruption the Be effusion cell temperature is adjusted to obtain a flux of 4×10^{11} cm^{-2} s^{-1}. The epitaxial layer sequence consists of 3000-Å Be-doped GaAs, 1000-Å undoped GaAs, the Be δ-doped layer, and a 1000-Å-thick GaAs top layer. Capacitance-voltage (*C-V*) measurements are performed with 250-μm radius Ti/Au (500 Å/1500 Å) Schottky contacts using a Hewlett-Packard Phase-Gain and Impedance Analyzer. Typical measurement frequencies are 1–2 MHz. Secondary-ion mass spectra (SIMS) are obtained from a Physical Elec-

[a] AT&T Bell Laboratories, Holmdel, New Jersey 07733.

Downloaded 25 Jun 2003 to 128.113.111.105. Redistribution subject to AIP license or copyright, see http://ojps.aip.org/japo/japcr.jsp

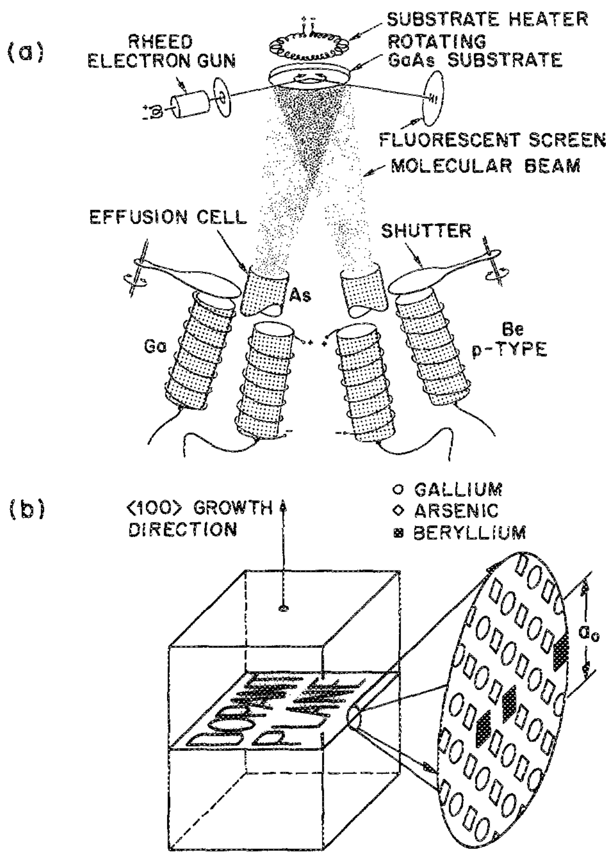

FIG. 1. (a) Schematic illustration of a molecular beam epitaxy system including effusion cells, shutters, and rotating substrate holder. (b) Schematic illustration of a δ-doped semiconductor. Dopants are confined to a highly doped plane, whose thickness is comparable to the lattice constant.

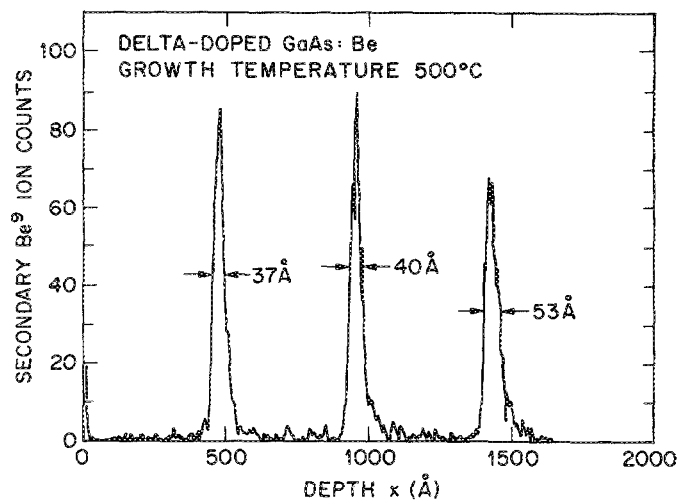

FIG. 2. SIMS profile of a Be-doped GaAs sample with three doping spikes at 500, 1000, and 1500 Å below the surface. The width of the profile increases with depth.

tronics "Phi 6300" system. The primary ion acceleration potential used is 3 kV. The raster diameter is 750 μm with 70% gated secondary ion detection. The crater depth is measured with a Dektak II depth profiler.

III. SPATIAL LOCALIZATION OF Be DOPANTS

SIMS and *C-V* profiling measurements are used to determine the degree of spatial localization of Be in δ-doped GaAs. It is shown that these techniques are very well suited to determine the degree of spatial localization of Be dopants in GaAs.

The SIMS doping profile of a sample containing three δ-doped spikes at 500, 1000, and 1500 Å below the GaAs surface is shown in Fig. 2. The concentration of each Be layer is $N_{Be}^{2D} = 4 \times 10^{12}$ cm^{-2}; and the growth temperature was 500 °C. The SIMS profile reveals three clearly resolved peaks at the anticipated depths of 500, 1000, and 1500 Å. The SIMS profile exhibits a full width half-maximum of 37 Å for the shallowest of the doped layers, which is the narrowest SIMS doping profile reported to date. The SIMS profile clearly indicates the strong spatial localization of Be in δ-doped GaAs grown at low substrate temperatures.

The resolution of SIMS profiles is limited by (i) roughening of the sputtered crater and (ii) the "knock-on effect." The roughening of the sputtered crater increases with sputtering time, which is illustrated by the increasing width of the SIMS peaks in Fig. 2. The second limitation of the SIMS resolution is given by the knock-on effect where sputtering primary ions transfer their momentum inelastically to Be dopants and causes Be atoms to be implanted deeper into the crystal. To minimize the knock-on effect a low acceleration potential of 3 kV is used in our measurements.

Taking into account both broadening mechanisms, we estimate the total broadening of the Be dopant profile to be less than 20 Å. Thus, δ-functionlike doping profiles can be obtained in Be-doped GaAs.

C-V profiles on samples with a single δ-doped layer below the surface confirm the SIMS results. A *C-V* profile measured at room temperature on a sample grown at $T_s = 500$ °C is shown in Fig. 3. The profile has a full width at half-maximum of 20 Å and is the narrowest *C-V* profile reported so far in GaAs.

For a correct interpretation of the *C-V* profile it is important to recall that the *C-V* measurement is based on a free-carrier effect rather than a dopant effect. The spatial resolution of *C-V* measurements is limited by the Debye screening length and the Thomas-Fermi screening length for nondegenerately and degenerately doped semiconductors and was discussed previously.[4] In semiconductor quantum structures the resolution of *C-V* profiles is given by the spatial extent of the ground-state wave function. In general, the dopant distribution is narrower than the measured *C-V* profiles. Thus, the *C-V* profile shown in Fig. 3 indicates a strongly spatially confined Be distribution.

From the *C-V* profiles measured on Be δ-doped samples we conclude that the total broadening of the Be-dopant profile is less 15 Å, in good agreement with the SIMS profiles.

IV. EFFECT OF ELEVATED SUBSTRATE TEMPERATURES

Elevated substrate temperatures of 580 and 660 °C are used to evaluate spatial spreading of dopants as a function of

Downloaded 25 Jun 2003 to 128.113.111.105. Redistribution subject to AIP license or copyright, see http://ojps.aip.org/japo/japcr.jsp

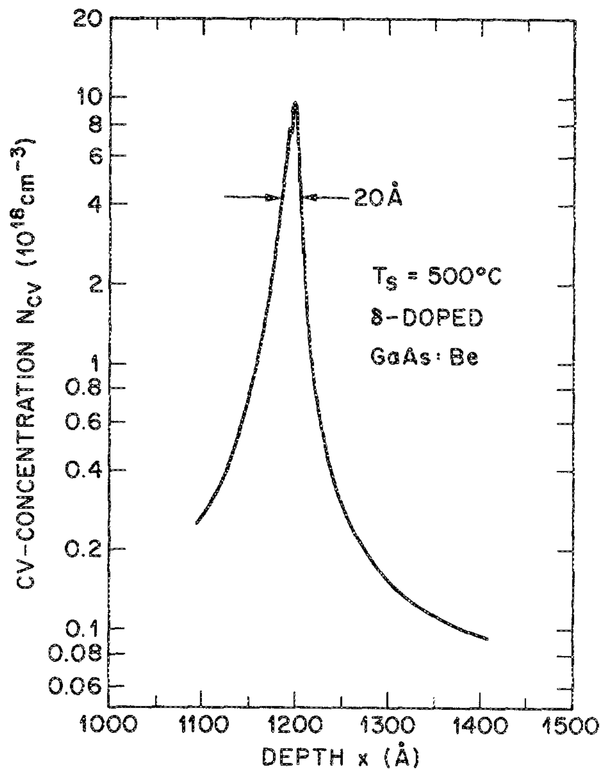

FIG. 3. Capacitance-voltage profile of a Be δ-doped GaAs sample grown at 500 °C by molecular beam epitaxy.

temperature. Such elevated temperatures result in stronger diffusion and, as will be discussed later, also enhanced segregation. Both, *C-V* profiles and SIMS profiles are used to monitor the spread of dopants at elevated substrate temperatures. *C-V* profiles of three samples grown at $T_s = 500$, 580, and 660 °C are shown in Fig. 4. The profiles indicate that δ-functionlike Be profiles can be obtained at 500 °C, while elevated temperatures $T_s \gg 500$ °C result in noticeable spreading of Be ions. At $T_s = 660$ °C the *C-V* profile broadens to 85 Å.

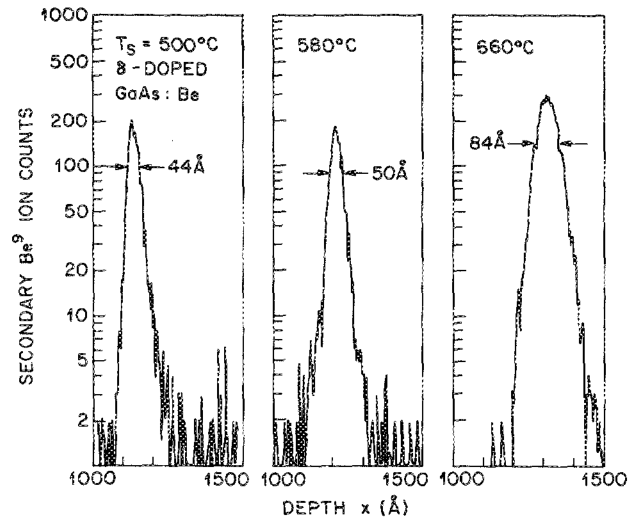

FIG. 5. SIMS profiles of three Be δ-doped GaAs epitaxial films grown at 500, 580, and 660 °C. The corresponding *C-V* profiles on the same samples are shown in Fig. 4.

The SIMS profiles shown in Fig. 5 are from the same set of samples and confirm the *C-V* profiles. An increasing spread of dopant ions becomes evident at elevated substrate temperatures. The individual spreading mechanisms such as diffusion and segregation will be discussed in subsequent sections.

The profiles in Figs. 4 and 5, which show the same three samples, allow us to compare the two profiling techniques. At small dopant spreads, the *C-V* technique yields narrower profiles, with superior resolution. As the spread of dopants increases at substrate temperatures of 660 °C, the resolution of *C-V* profiles and SIMS profiles is comparable. This can be explained by the fact that the limits of the SIMS resolution are concentration independent. In contrast, since the *C-V* profile resolution (Debye or Thomas-Fermi screening length) is concentration dependent, the widths of *C-V* pro-

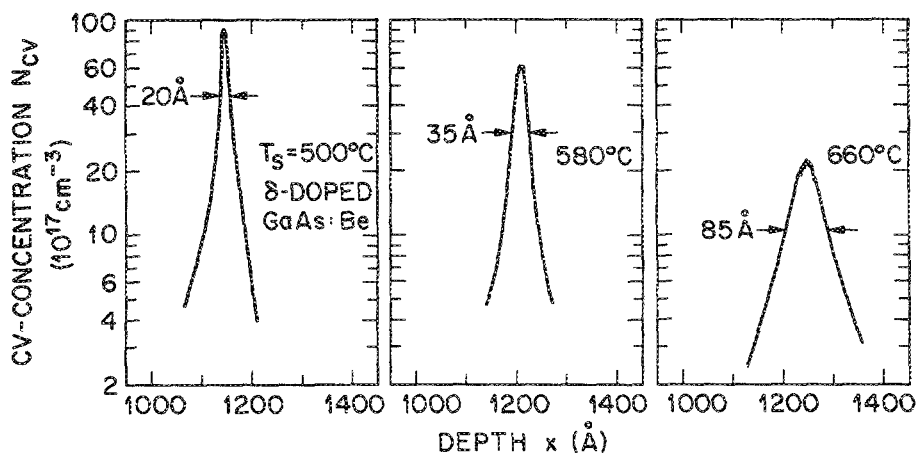

FIG. 4. Capacitance-voltage profiles of three Be δ-doped GaAs epitaxial films grown at 500, 580, and 660 °C.

Downloaded 25 Jun 2003 to 128.113.111.105. Redistribution subject to AIP license or copyright, see http://ojps.aip.org/japo/japcr.jsp

files are expected to track the SIMS profile widths at increased spread (i.e., decreased concentration).

V. DIFFUSION OF Be IN GaAs

The diffusion coefficient of Be in GaAs is determined by *C-V* profiling of samples rapidly annealed at temperatures of 600–1000 °C. The GaAs sample used for the experiment was grown at a low growth temperature (500 °C) and has a profile width of 20 Å before annealing, indicating the absence of significant diffusion during growth. After annealing the samples, AuGe/Ni/Au ohmic contacts and Ti/Au Schottky contacts are evaporated for the capacitance measurement. The profiles of the samples annealed for 5 s at different temperatures are shown in Fig. 6. A systematic decrease in the peak concentration as well as an increase in width up to 440 Å is observed with increasing annealing temperature. The increasing width of the *C-V* profiles allows us to determine the approximate diffusion length associated with each annealing temperature using the relation

$$\sigma^2 = \sigma_{\rm diff}^2 + \sigma_i^2, \qquad (1)$$

where σ_i represents the half-width at half-maximum of the *C-V* profile in the absence of diffusion ($\sigma_i \cong 10$ Å) and $\sigma_{\rm diff}$ is the diffusion-induced broadening of the *C-V* profile such that the total half-width of the profile is σ.

Diffusion is an initially δ-functionlike dopant profile located at $z = 0$ results in a Gaussian dopant distribution with

$$N_D(z) = \frac{N_D^{\rm 2D}}{\sigma\sqrt{2\pi}} \exp\left[-\frac{1}{2}\left(\frac{z}{\sigma}\right)^2\right]. \qquad (2)$$

The diffusion length is defined as $L_D = \sqrt{D\tau}$ and is related to the standard deviation of the Gaussian distribution by

$$L_D = \sqrt{D\tau} = \sigma/\sqrt{2}, \qquad (3)$$

where τ is the time the sample is subjected to annealing.

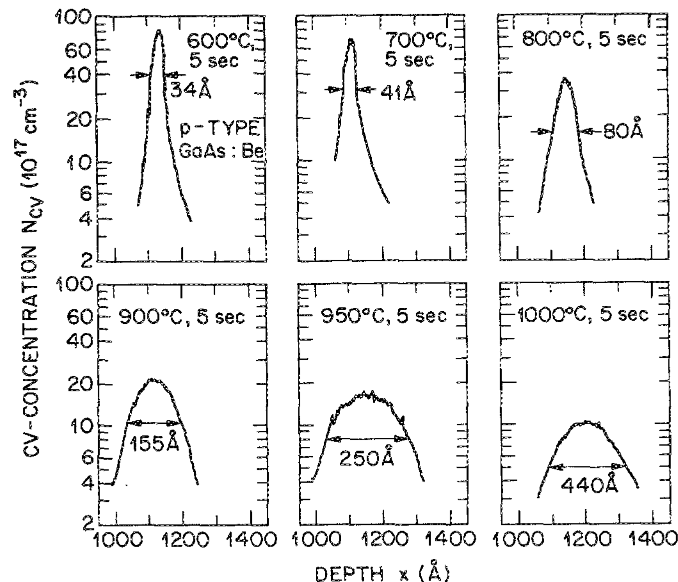

FIG. 6. Capacitance-voltage profiles of a Be δ-doped GaAs sample grown at 500 °C and subjected to post-growth anneal at 600, 700, 800, 900, 950, and 1000 Å for 5 s.

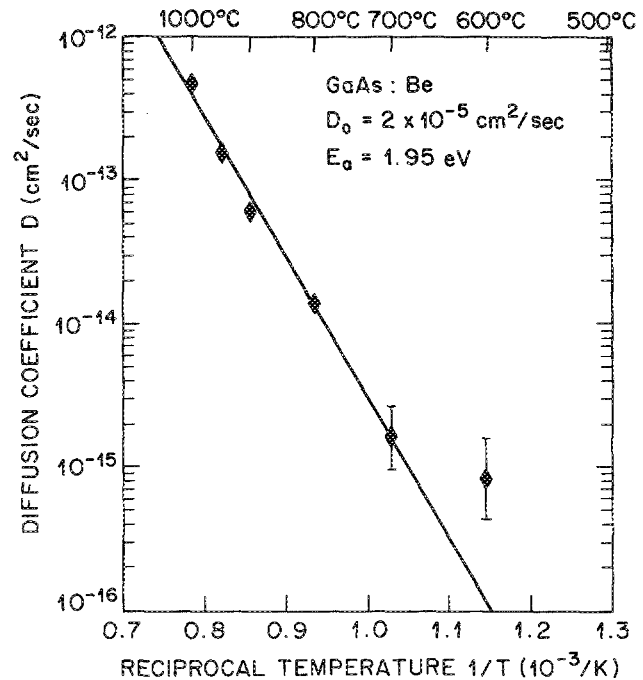

FIG. 7. Diffusion-coefficient of Be in GaAs as a function of reciprocal temperature. The activation energy and the corresponding D_0 are determined.

The diffusion coefficient of Be in GaAs is displayed in Fig. 7 for temperatures of 600–1000 °C. If the temperature-dependent diffusion coefficient is given by the exponential relation:

$$D = D_0 \exp(-E_a/kT), \qquad (4)$$

then the experimental points are described best by an activation energy $E_a = 1.95$ eV and a $D_0 = 2\times10^{-5}$ cm^2/s.

The diffusion coefficient of Be in GaAs found is more than two orders of magnitude smaller than the Be diffusion coefficient determined previously.[5] We note, however, that the Be concentrations used are much lower than the concentrations used previously. As will be shown later, other effects play an important role at high concentrations in addition to simple diffusion. The diffusion coefficient illustrated in Fig. 7 is therefore more realistic.

VI. SEGREGATION OF Be DURING GaAs GROWTH

Segregation of Be dopants during growth represents an additional broadening mechanism of Be δ-doped structures. The term "segregation" will be used for the movement of dopants predominantly towards the surface during crystal growth. We will show that surface segregation can be consistently explained by Fermi-level pinning at the semiconductor-vacuum interface, which results in the formation of a dipole layer consisting of positively charged surface states and the negatively charged Be acceptor layers. We show that this mechanism causes surface segregation for *all* impurities in III-V semiconductors.

Downloaded 25 Jun 2003 to 128.113.111.105. Redistribution subject to AIP license or copyright, see http://ojps.aip.org/japo/japcr.jsp

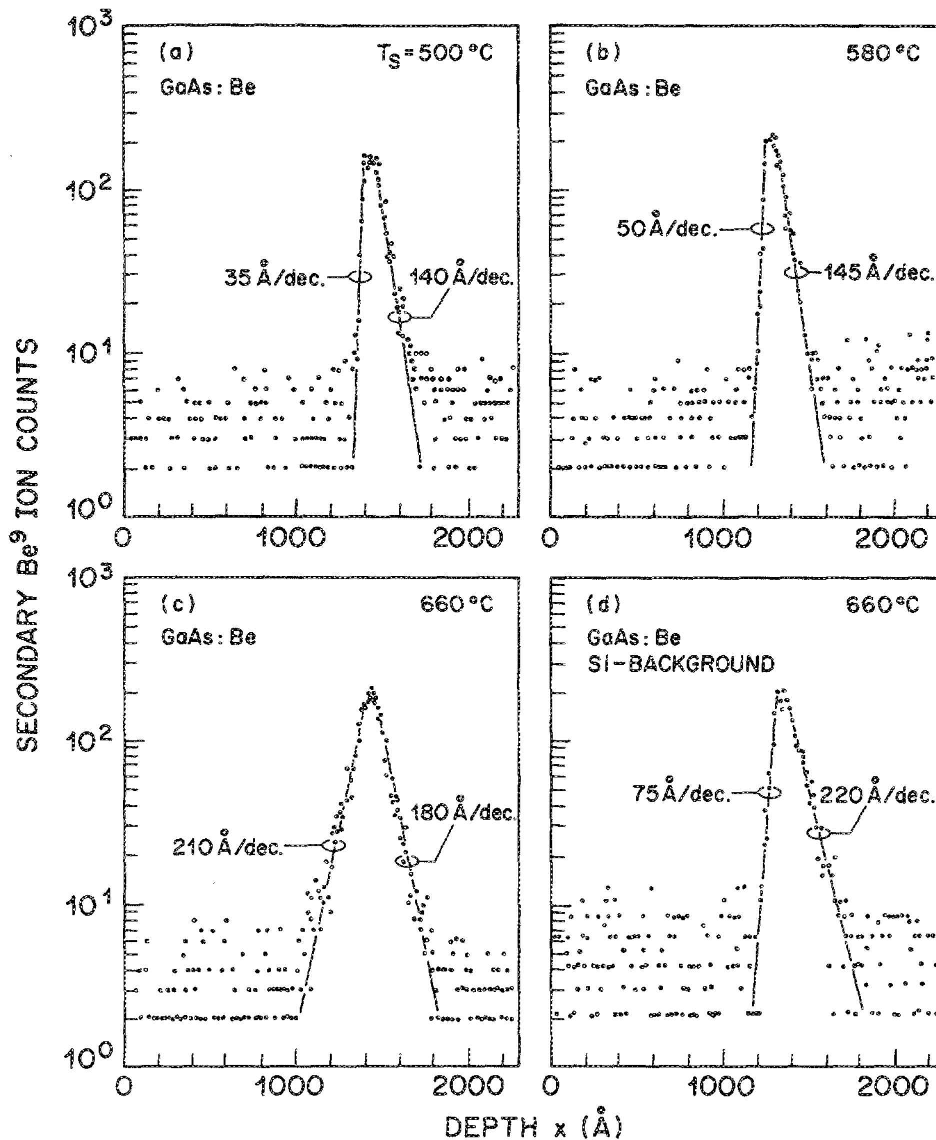

FIG. 8. SIMS profiles of Be δ-doped GaAs grown at (a) 500, (b) 580, and (c) 660 °C. At low substrate temperatures, the SIMS profile is asymmetric due to the "knock-on" effect. At elevated substrate temperatures (e.g., 660 °C), clear surface segregation becomes evident. (d) Surface segregation is greatly reduced (at 660 °C) if Si background doping is included, which reverses and screens the surface electric field.

Surface segregation of Be in GaAs becomes obvious in the SIMS profiles illustrated in Fig. 8. At low substrate temperatures [Fig. 8(a)], no surface segregation occurs and the SIMS profile is asymmetric due to the well-known knock-on effect. As a consequence, the trailing slope (140 Å/decade) is not as steep as the leading slope (35 Å/dec). At an increased substrate temperature of 580 °C [Fig. 8(b)], the leading slope changes more rapidly (50 Å/dec) as compared to the trailing slope (145 Å/dec). However, at a growth temperature of 660 °C surface segregation becomes obvious as the leading slope is less steep (210 Å/dec) as compared to the trailing slope (180 Å/dec). The asymmetry is even stronger than suggested by Fig. 8(c) since the knock-on effect always tends to broaden the SIMS profile towards the substrate side. We find the same qualitative tendency for Si in GaAs and Si in $Al_xGa_{1-x}As$.[12]

Before we turn to the physical explanation of Be surface segregation, we show that Be segregation can be reversed (i.e., dopants move towards the substrate side) by appropriate Si-background doping. The sample containing such a background doping was also grown at 660 °C. It contained both below and above the Be δ-doped layer, two, 1000-Å-thick heavily Si-doped regions, each with a concentration of $N_{Si} = 4\times 10^{18}$ cm^{-3}. The Be SIMS result of this sample is shown in Fig. 8(d), which shows that Be segregation is strongly reduced. Rather than surface segregation, the SIMS profile strongly suggests that Be dopants have migrated toward the substrate, as indicated by the long trailing tail of slope 220 Å/dec and the steep leading edge of slope 75 Å/dec. The asymmetry of this spectrum can be explained, only if we assume that Be dopants migrated toward the substrate (reversed surface segregation).

We will now propose a model based on Fermi-level pinning,[6] which can explain the segregation of Be in GaAs and

Downloaded 25 Jun 2003 to 128.113.111.105. Redistribution subject to AIP license or copyright, see http://ojps.aip.org/japo/japcr.jsp

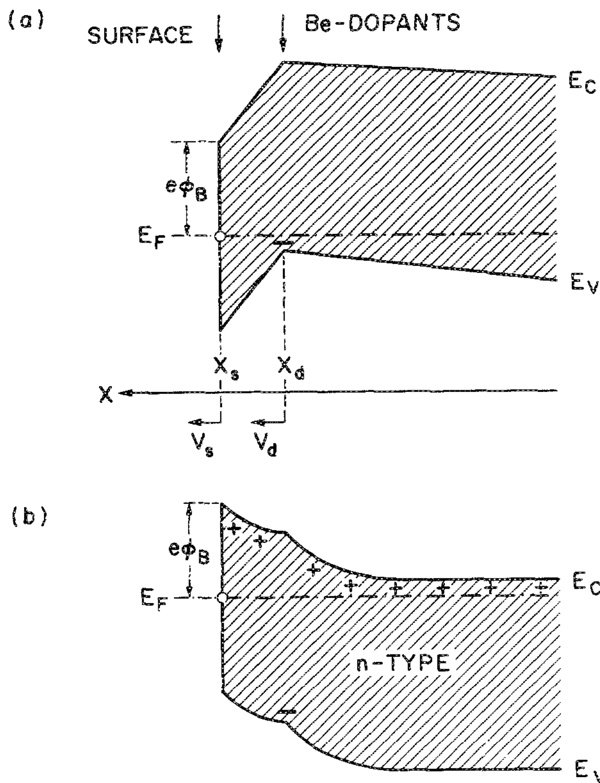

FIG. 9. Explanation of the segregation effect. (a) Band diagram of a growing semiconductor with the Fermi level pinned at energy $e\phi_B$ below the conduction band minimum. The surface moves at the growth velocity v_s. The dipole interaction between negative acceptors and holes in surface states result in migration of dopants toward the surface with a velocity v_s. (b) Renewal of the surface electric field by n-type background doping.

its reversal. We will first neglect any diffusion effects and consider only segregation. The band diagram of a semiconductor containing a δ-functionlike doping profile is shown in Fig. 9(a). Figure 9(a) shows that inclusion of appropriate background doping results in reversal of the surface electric field, which represents a driving force for impurities toward the substrate.

The surface of the semiconductor is assumed to be moving along the x direction with a velocity v_s. For a two-dimensional doping density of N_A^{2D} the electric field of the dipole is given by

$$\mathbf{E} = eN_A^{2D}/\epsilon, \tag{5a}$$

$$\mathbf{E} = (E_g - \phi_B)/(x_s - x_d), \tag{5b}$$

where e is the elementary charge, ϵ is the permittivity of the semiconductor and $x_s = v_s t$ and x_d are the position of the surface and the doped layer, respectively. Equation (5a) is valid if the doped layer is depleted of all free carriers, i.e.,

$$x_s - x_d \leqslant (E_g - \phi_B)\epsilon/eN_A^{2D},$$

while Eq. (5b) is valid if the doped layer is partly depleted of free carriers, i.e.,

$$x_s - x_d \geqslant (E_g - \phi_B)\epsilon/eN_D^{2D}.$$

The segregation velocity of dopants in the electric field is given by

$$v_d = \frac{dx_d}{dt} = \mu \mathbf{E}, \tag{6}$$

where μ is the doping ion mobility which can be obtained from the diffusion coefficient of Be in GaAs and the Einstein relation $\mu = D\,e/kT$. (The Be diffusion coefficient is shown in Fig. 7.)

For small distances between the doped layer and the surface, the dipole field is given by Eq. (5a) and the segregation velocity of the dopants is given by

$$v_d = \frac{De}{kT}\frac{eN_A^{2D}}{\epsilon}. \tag{7}$$

At 500 °C the diffusion coefficient $D < 10^{-16}$ cm^2/s yields [see Eq. (7)] a negligible segregation velocity. However, at $T = 660$ °C one obtains $D \cong 10^{-15}$ cm^2/s where the segregation velocity is 0.7 Å/s, which is comparable in magnitude to the growth velocity (v_g) of GaAs of 0.9 μm/h = 2.5 Å/s. We see that the segregation velocity has the same order of magnitude as the growth rate. Thus, significant segregation is expected to occur at $T = 660$ °C.

To obtain a single differential equation for small $(x_s - x_d)$ and large $(x_s - x_d)$ the electric field given in Eqs. (5a) and (5b) is approximated by

$$\mathbf{E} = \left[\left(\frac{e}{\epsilon}N_A^{2D}\right)^{-1} + \left(\frac{E_g - \phi_B}{x_s - x_d}\right)^{-1}\right]^{-1}. \tag{8}$$

This field approaches the exact field of Eqs. (5a) and (5b) for

$$x_s - x_d \lll (E_g - \phi_B)\epsilon/N_D^{2D}$$

and

$$x_s - x_d \ggg (E_g - \phi_B)\epsilon/N_D^{2D},$$

respectively. The field represents a lower limit of the true field in the intermediate range. The differential equation then becomes

$$\frac{dx_d}{dt} = \frac{De}{kT}\left(\frac{\epsilon}{eN_A^{2D}} + \frac{x_s - x_d}{E_g - \phi_B}\right)^{-1}, \tag{9}$$

with $x_s = v_s t$. [Note that diffusion is neglected in Eq. (8).] This equation is solved numerically for the three growth temperatures 500, 580, and 660 °C. For the calculation, the experimental carrier density of $N_A^{2D} = 4 \times 10^{12}$ cm^{-2} and a total growth time after the deposition of the doped layer of $t = 280$ s are used.

The segregation length is estimated by solving the nonlinear differential Eq. (9). The results of the numerical solution are as follows: At low substrate temperature of 500 °C the segregation during growth of the 1000-Å-thick top layer is 0.25 Å. The corresponding calculated segregation length at the growth temperatures of 580 and 660 °C are 3.5 and 33 Å, respectively. These calculated segregation lengths are in good qualitative agreement with the experimental results displayed in Fig. 8.

These approximate calculations allow us to estimate the relative importance of the diffusion and the segregation process. The diffusion length is known to equal $\sqrt{Dt}$. According to Eq. (8), the segregation length is proportional to Dt (where we assume that the field-term is independent of t).

Downloaded 25 Jun 2003 to 128.113.111.105. Redistribution subject to AIP license or copyright, see http://ojps.aip.org/japo/japcr.jsp

Since D depends exponentially on temperature, diffusion ($\sqrt{Dt}$) dominates at low temperatures, while segregation (Dt) dominates at higher temperatures; this trend is clearly confirmed by our experiments.

The calculation above, although it gives a very good explanation of the physical process causing surface segregation, is unrealistic in two respects. First, since diffusion of impurities is neglected, the impurity profile remains δ-functionlike. Inclusion of diffusion in the calculation would naturally broaden the dopant profile.

The second insufficiency of the calculation is the omission of screening. At the growth temperature of 660 °C the concentration of thermally excited, intrinsic carriers reaches a value of $n_i \cong 10^{16}$ cm^{-3}. This concentration corresponds to a Debye screening length of ≅550 Å.

The understanding of the segregation mechanism opens up new ways to either make use of the mechanism or to avoid segregation in these semiconductors. The possible uses include the controlled field-driven redistribution of dopants close to the surface. On the other hand, possibilities to reduce the segregation include (i) high intensity illumination of the growing surface to increase the free carrier density and the screening, (ii) growth on different surface orientations such as the (110) plane on which the Fermi-level pinning is reduced, and (iii) growth at low temperatures at which segregation is less pronounced.

VII. HIGH-DOPING REGIME

In this section, we investigate the high-doping regime of Be δ-doped GaAs. We show that significant spread occurs at high-doping concentrations and explain the spread in terms of electrostatic repulsion of dopants. Dopant correlation effects were not taken into account previously and result in a correlated, nonrandom dopant distribution.

Naively, one would assume that the free carrier concentration equals the doping concentration in doped materials. However, it was shown earlier that the free electron concentration saturates at about $1\text{–}2\times10^{13}$ cm^{-2} for n-type Si δ-doped GaAs.[7] The highest electron concentrations achieved were 2×10^{13} cm^{-2}.[8,9]

The hole concentration (measured by Hall effect at 300 K) of six Be δ-doped GaAs samples is shown in Fig. 10 as a function of deposition time. The solid line represents the best linear fit of Be-deposition time (i.e., growth interruption time) and hole concentration. From the slope of the line we infer a Be-deposition rate of 4×10^{11} cm^{-2} s^{-1}. The substrate temperature during growth suspension and during growth of the 1000-Å-thick top layer was 500 °C.

Most surprisingly, the free-hole concentration depicted in Fig. 10 shows no indication of saturation but follows the Be deposition in a linear fashion. The highest measured hole concentration is 6.6×10^{14} cm^{-2}, the concentration of a single cation (Ga) monolayer.

The hole mobility as inferred from Hall measurements at room temperature and at $T=60$ K is shown in Fig. 11 as a function of the two-dimensional hole concentration. The mobility decreases steadily with increasing hole concentration and reaches a value of 50 cm^2/V s at 300 K for the

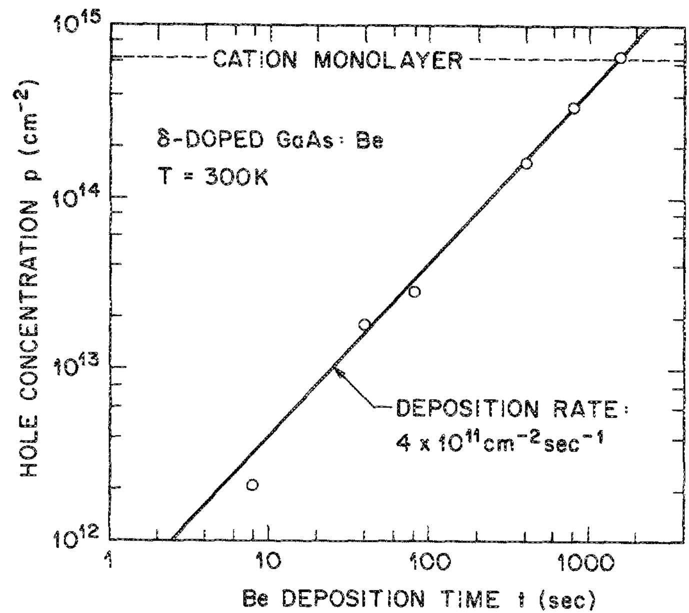

FIG. 10. Hole concentration at room temperature vs Be-deposition time. The straight line represents a deposition rate of 4×10^{11} cm^{-2} s^{-1}.

highest concentration. The mobility data do not indicate any deterioration of transport characteristics at high concentrations. This is corroborated by the featureless surface morphology of the samples.

Significant spreading of Be in δ-doped GaAs occurs at high dopant concentrations. Figure 12 shows the SIMS profiles of the same six GaAs samples. The three samples of lower concentration (nominal Be concentration $\leqslant 2\times10^{13}$ cm^{-2}) exhibit good spatial localization of dopants, as indicated by the narrow width of the three SIMS profiles, which are smaller than 50 Å. However, as the concentration increases, the SIMS profiles broaden dramatically, as inferred

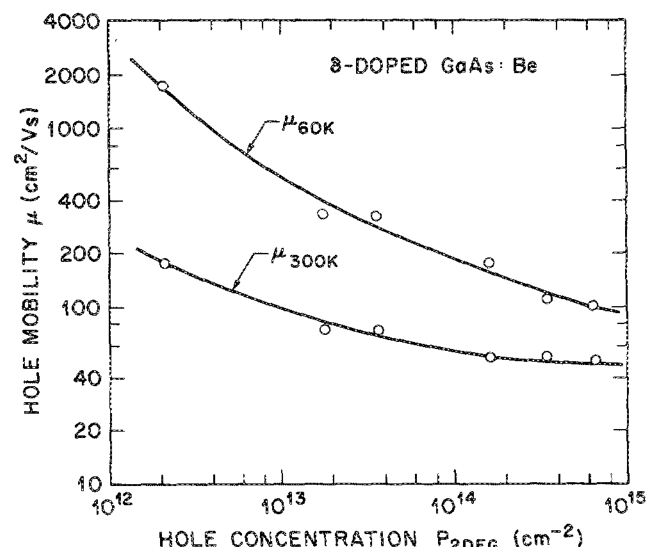

FIG. 11. Hall mobility of holes in Be δ-doped GaAs vs carrier concentration at $T=60$ and 300 K.

Downloaded 25 Jun 2003 to 128.113.111.105. Redistribution subject to AIP license or copyright, see http://ojps.aip.org/japo/japcr.jsp

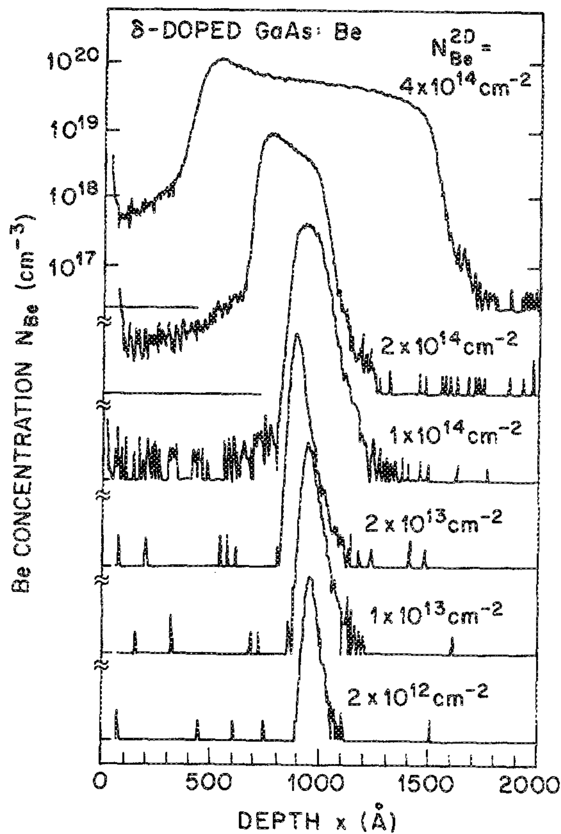

FIG. 12. Be concentration of δ-doped GaAs for different Be concentrations. Below a concentration of 10^{14} cm^{-2}, Be is spatially localized, i.e., δ-functionlike doping profiles are possible. At higher concentration, significant spread is observed.

from Fig. 12. Such doping profiles can certainly not be considered to be δ functionlike.

The spread of dopants at high concentrations can be explained by a concentration-dependent diffusion coefficient. However, we propose an alternative mechanism based on electrostatic repulsion of ionized Be dopants, which explains our results consistently. It was previously suggested, that Be has a concentration dependent diffusion coefficient with D increasing rapidly, as the Be concentration exceeds 10^{19} cm^{-3}. Such a concentration dependence can be explained by degradation of material quality, i.e., an increasing concentration of defects, which facilitate diffusion processes. A second explanation is enhanced Be-pair formation at high Be concentrations. Be pairs are expected to diffuse more easily as compared to atomic Be.[10] However, we find no indication of an increased defect concentration or the formation of compensated Be pairs. Such defects or Be pairs would reduce the free carrier concentration as well as the mobility. A reduction of either free carrier concentration or mobility is not indicated by the transport (Hall) results. We therefore propose that repulsive Coulomb interaction of ionized Be dopant acts as a driving force to spread dopants out of the thin, highly doped sheet. At low concentrations, the mean dopant-to-dopant separation is large, and Coulomb interaction is insignificant. [At $N_A^{2D} = 5\times10^{12}$ cm^{-2} the mean distance between Be dopants is approximately $d = (N_A^{2D})^{-1/2} \cong 50$ Å.] However, at higher Be concentrations the mean Be separation could be as small as $\frac{1}{2}\sqrt{2}a_0 \cong 4$ Å, i.e., the distance of two cation sites. Such small separations lead to significant Coulomb interaction. We support the claim of strong repulsive Coulomb interaction with the following simple calculation, which does not employ any fitting parameter.

In the following calculation we estimate the drift of two closely separated ionized dopants due to Coulomb repulsion. If two Be dopants occupy two adjacent cation sites their separation is $r_0 = \sqrt{2}a_0/2$. Both dopants drift with a velocity:

$$v = \frac{dr}{dt} = \mu \mathrm{E}, \tag{10}$$

in opposite directions due to Coulomb repulsion. The drift mobility of the dopant μ is estimated from the Einstein relation:

$$\mu = D(e/kT) \tag{11}$$

and the Coulomb electric field $\mathbf{E}$ is given by

$$\mathbf{E} = e/4\pi\epsilon r^2. \tag{12}$$

Insertion of Eqs. (11) and (12) into Eq. (10) and taking into account that *both* dopants drift at velocity v, yields the differential equation

$$\frac{1}{2}\frac{dr}{dt} = D\frac{e}{kT}\frac{e}{4\pi\epsilon r^2}, \tag{13}$$

which can be solved by separation of variables. One obtains

$$r(t) = \left(6\frac{De}{kT}\frac{e}{4\pi\epsilon}t - r_0^3\right)^{1/3}, \tag{14}$$

which is the distance of the two dopants as a function of time. To estimate the distance of two dopants due to drift occurring at low growth temperatures, we choose the parameters $T = 500$ °C, $r_0 = 4$ Å, $D = 10^{-17}$ cm^2/s, and $t = 300$ s. The time t corresponds to the experimental growth time used for the 1000-Å-thick layer on top of the δ-doped layer. As a result one obtains for the separation $r(300\text{ s}) \cong 14$ Å. That is, initially closely spaced dopants drift 14 Å in opposing directions due to Coulombic repulsion.

Certainly, conventional diffusion, i.e., the random movement of dopants occurs simultaneously. The pure diffusion length can be estimated to be $L_D = \sqrt{D\tau} \cong 5$ Å for the same diffusion coefficient and time. Thus, it is obvious that drift rather than diffusion dominates at the extremely high-doping concentrations used in this study. We point out that the occurrence of drift could be misinterpreted as an enhancement of the diffusion coefficient at high-doping concentrations.

The occurrence of drift also represents a fundamental limit for the highest Be-doping concentration achievable in GaAs. Assuming that the average distance between dopants is at least 14 Å, as inferred from the drift calculation, the highest achievable three-dimensional concentration would be at the most $N_A = d^{-3} = 3.6\times10^{20}$ cm^{-3}. A concentration of the same order of magnitude is indeed found experimentally, as indicated by the SIMS profiles of Fig. 12.

The above considerations raise the question, how can the highest Be concentration in GaAs be increased? The an-

Downloaded 25 Jun 2003 to 128.113.111.105. Redistribution subject to AIP license or copyright, see http://ojps.aip.org/japo/japcr.jsp

swer to this question is straightforward. If Coulomb repulsion effects, and the resulting drift, is the limiting factor in getting high Be concentrations, then a further lowering of the growth temperature to, e.g., 400 °C, reduces the diffusion coefficient and, via the Einstein relation, also the drift mobility.

In order to study the high-doping regime of Be, a Be δ-doped GaAs sample was grown at 400 °C. Figure 13(a) and 13(b) show the SIMS profiles of GaAs samples doped during growth interruption with Be of concentration $N_{Be}^{2D} = 4\times10^{14}$ cm^{-2}. The growth temperature was 400 and 500 °C for the profiles displayed in Fig. 13(a) and 13(b), respectively. The sample grown at 400 °C shows less spatial spreading and a higher peak concentration as compared to the sample grown at 500 °C. The peak concentration is 2.3×10^{20} cm^{-3}, which is the highest Be doping reported for GaAs. It is expected that higher concentrations can be achieved at even lower growth temperatures. Similar observations were made in $Ga_{0.47}In_{0.53}As$ by Hamm *et al.*[11]

VIII. NONRANDOM DISTRIBUTION OF DOPANTS AT HIGH DOPANT CONCENTRATION

The Coulomb-interaction arguments used in the previous section suggested that correlation effects lead to deviations from random dopant distribution in semiconductors. We pointed out previously that the random dopant distribution fails to be a valid assumption at high dopant distributions.[12] In this section we will estimate the deviation of the dopant distribution from the random distribution. The calculation follows the same concept used previously by Shockley.[13] We will show that deviations from the random dopant distributions are expected at high dopant concentrations. The calculation will be carried out for a homogeneously doped (not a δ doped) semiconductor.

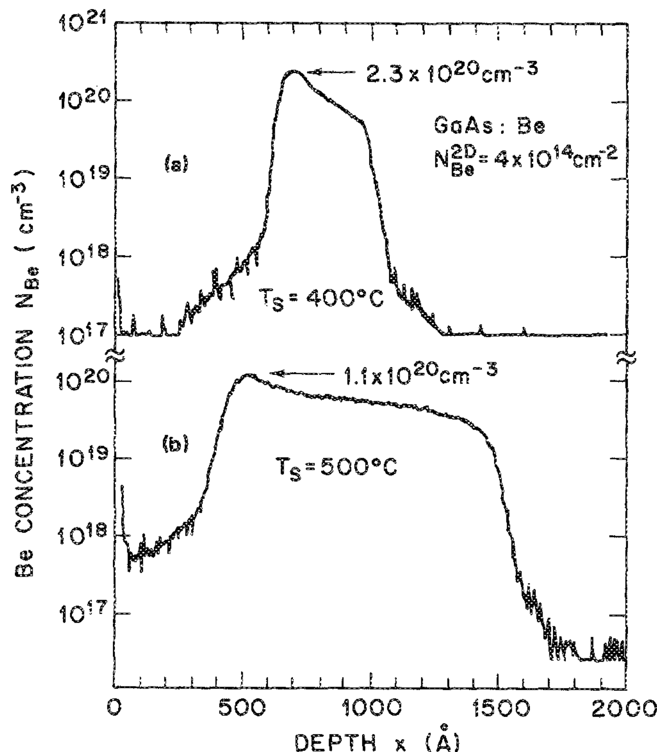

FIG. 13. SIMS profile of Be δ-doped GaAs grown at (a) $T_s = 400$ °C and (b) $T_s = 500$ °C. The maximum concentration achieved is 2.3×10^{20} cm^{-3} at the low growth temperature.

Enhanced electron mobilities were found in δ-doped GaAs, as compared with homogeneously doped material.[8] The magnitude of the mobility enhancement was a maximum of a factor of 4. The improved transport characteristics were attributed to (i) high degeneracy, (ii) spatial electron-dopant separation, and (iii) screening. Further improvement of mobilities is expected if the dopant distribution is nonrandom.

Recently, Headrick *et al.*[14] reported *B* monolayers in [111] Si which were completely ordered in a $\sqrt{3}\times\sqrt{3}$ surface reconstruction. In addition, theoretical considerations of Levi *et al.*[15] showed that elastic scattering is reduced in semiconductors with nonrandom dopant distributions.

To facilitate the calculation of the potential energy in semiconductors, we assume that dopants occupy the sites of a simple cubic lattice, but their concentration varies spatially, as indicated in Fig. 14. Areas of high ionized dopant concentration also represent areas of high potential energy. Areas of lower concentration have a smaller electrostatic energy. If dopants were randomly distributed, and their average concentration were N_A, then the probability of A dopants being in a volume V is given by the Poisson probability distribution

$$p(A) = (N^A/A!)e^{-N}, \quad (15)$$

where $N = N_D V$ is the average number of dopants within the volume V. For large N the Poisson distribution can be approximated by a Gaussian distribution, which facilitates the following calculation. The Gaussian distribution then has the variance $\sigma^2 = N$ and the expectation value N:

$$p(A) = \frac{1}{\sqrt{2\pi N}} \exp\left[-\frac{1}{2}\left(\frac{A-N}{\sqrt{N}}\right)^2\right]. \quad (16)$$

This distribution is shown in Fig. 15 by the solid curve for

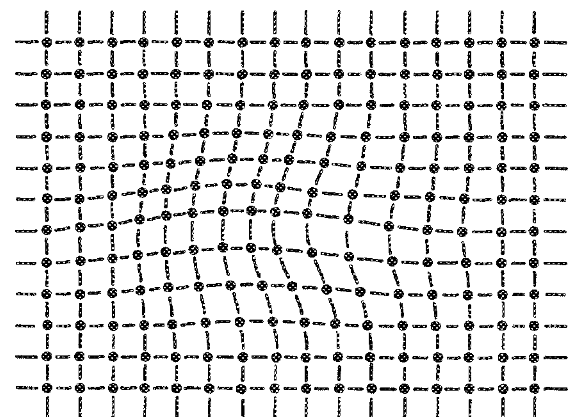

FIG. 14. Simplified illustration of random dopant distribution, in which the density of dopants varies spatially.

Downloaded 25 Jun 2003 to 128.113.111.105. Redistribution subject to AIP license or copyright, see http://ojps.aip.org/japo/japcr.jsp

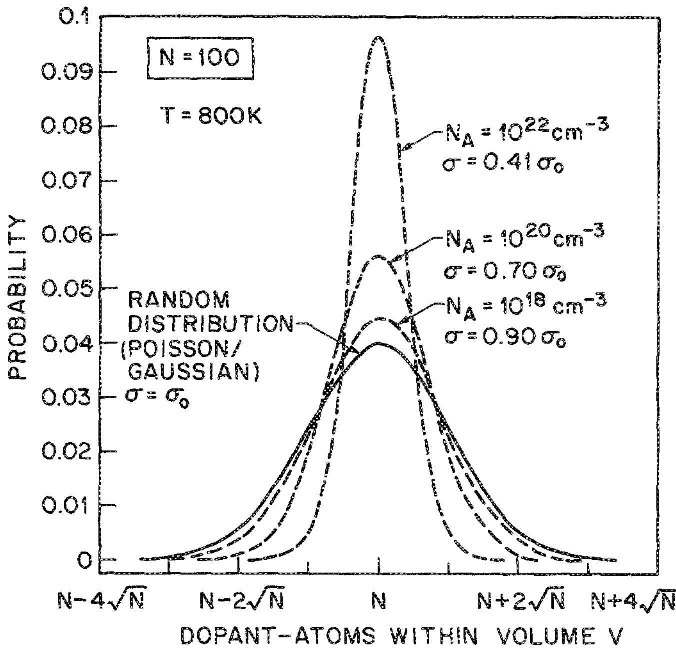

FIG. 15. Random (solid line) and nonrandom (dashed lines) dopant distributions. The ordinate shows the probability of finding A dopant atoms in a volume in which the average $N = 100$ dopants are situated. At high-doping concentrations the distribution becomes narrower, due to repulsive Coulomb interaction.

$N = 100$. The exponential term of the Gaussian distribution corresponds to the entropy term, $\exp(TS/kT) = \exp(S/K)$ in a calculation based on statistical mechanics.[11] The potential energy of the repulsive dopants of charge e is given by

$$E = \frac{1}{2} \sum_{i \neq j} \frac{e^2}{4\pi\epsilon r_{ij}}. \tag{17}$$

This energy is reminiscent of the Madelung energy in ionic crystals. The potential energy is minimized if the dopants are ordered in a face-centered cubic lattice. However, it is very unlikely that such a minimum energy configuration will be achieved. For simplicity, we assume that dopants are rather in a simple cubic lattice with the distance between dopants being $d = N_A^{-3}$. While the volume of an ordered impurity lattice contains N ions, different volumes may contain $N \pm \sqrt{N}$ ions for a random dopant distribution. The mean distance then changes by

$$\sigma_d = \pm \tfrac{1}{3} N^{-5/6} V^{1/3}. \tag{18}$$

The introduction of the dimensionless parameter:

$$\lambda = (A - N)/\sqrt{N}, \tag{19}$$

allows one to change continuously from the ordered ($\lambda = 0$) to the random ($\lambda = 1$) distribution of dopant ions. The relative displacement is then given by

$$\sigma_d/d = \pm \tfrac{1}{3} \lambda^2 N^{-1/2}. \tag{20}$$

If a dopant atom is displaced by σ_d in the directions of the three Cartesian coordinates, the mean increase of potential electrostatic energy (only next neighbors considered) is given by

$$\sigma_{E,i} = 3\left[\frac{1}{2}\left(\frac{e^2}{4\pi\epsilon(d+\sigma_d)} + \frac{e^2}{4\pi\epsilon(d-\sigma_d)}\right) - \frac{e^2}{4\pi\epsilon d}\right] = 3\frac{e^2}{4\pi\epsilon}\frac{1}{d}\left(\frac{\sigma_d}{d}\right)^2. \tag{21}$$

Thus, the mean separation between dopants d and its standard deviation σ_d, are related to the electrostatic energy of a dopant ion. Within a volume V, the random distribution has an energy which is higher than the ordered distribution. The additional energy due to the randomness of dopants is given by

$$\sigma_{E,N} = (e^2/12\pi\epsilon) N_A^{1/3} \lambda^2. \tag{22}$$

Under conditions close to thermal equilibrium, the energies corresponding to different doping distributions can be assumed to be distributed according to the Boltzmann distribution

$$p(A) \sim \exp - \sigma_E/kT. \tag{23}$$

The effect of the Boltzmann tail is to reduce the probability of configurations which are very dense (i.e., configurations of high electrostatic energy). Combination of the Boltzmann distribution with the entropy factor of the Gaussian distribution yields after renormalization

$$p(A) = \frac{1}{\sqrt{2\pi N}} \sqrt{1 + \frac{e^2 N_A^{1/3}}{6\pi\epsilon kT}} \times \exp\left[-\frac{(A-N)^2}{2N}\left(1 + \frac{e^2 N_A^{1/3}}{6\pi\epsilon kT}\right)\right]. \tag{24}$$

For dilute doping concentrations ($N_D \ll 10^{18}$ cm^{-3}) the potential energy does not change the random distribution (solid line in Fig. 15). However, at high-doping concentrations significant deviations from the random Poisson distribution are expected. The modified distribution is influenced by dopant correlation effects, i.e., by repulsive interactions between ionized dopants. Dopant configurations with very small distances between dopants (which have a finite probability for the random distribution) are unlikely due to repulsive interactions. It is worthwhile to note, that screening is of minor influence, since the Thomas–Fermi screening length exceeds the inter-particle distance at high-doping concentrations.

The above calculation applies to homogeneously doped semiconductors. For δ-doped semiconductors, the consequences of the Coulomb correlation effects are twofold. First, impurities tend to repel one another in the impurity plane, leading to a more equidistant impurity distribution. Second, the correlation effect tends to drive impurities out of the original impurity plane, i.e., results in a wider (not δ-functionlike) impurity distribution. Such a wider impurity distribution is indeed observed experimentally at high Be concentrations as shown in Fig. 12.

IX. CONCLUSIONS

Capacitance-voltage (C-V) and secondary ion mass spectroscopy (SIMS) measurements on Be δ-doped GaAs grown by molecular beam epitaxy reveal that Be is spatially localized to within a few lattice constants (< 20 Å) at low growth temperatures and concentrations $< 10^{14}$ cm^{-2}. C-V

Downloaded 25 Jun 2003 to 128.113.111.105. Redistribution subject to AIP license or copyright, see http://ojps.aip.org/japo/japcr.jsp

and SIMS profiles with a full width at half-maximum of 20 and 37 Å are the narrowest profiles ever achieved on Be-doped GaAs. Both techniques are in good agreement. Elevated substrate temperatures result in a clear spread of Be dopants. The broadening of the Be-doping profile is explained by (i) Fermi-level pinning-induced segregation, (ii) repulsive Coulomb interaction of dopants, and (iii) diffusion. The diffusion coefficient of Be in GaAs is determined. Furthermore, we show that the highest three-dimensional Be concentrations are achieved at low growth temperatures and exceed 2×10^{20} cm^{-3}. This concentration is limited by repulsive Coulomb interaction, which leads to significant drift of dopants. The drift at high concentration can be understood as the physical basis of an enhanced diffusion coefficient of Be in GaAs. It is shown theoretically, that the repulsive Coulomb interaction leads to a nonrandom, strongly correlated dopant distribution.

Note added in proof. The authors thank R. B. Beall and J. J. Harris for making available experimental results prior to publication. Recently, Ourmazd *et al.* [Appl. Phys. Lett. (in press)] studied the spatial localization of Be in GaAs by means of transmission electron microscopy. They found that Be impurities are spread over a length of $\leqslant 15$ Å.

ACKNOWLEDGMENTS

The authors thank J. E. Cunningham, L. C. Feldman, A. S. Jordan, A. Ourmazd, and M. B. Panish for valuable discussions.

[1] S. J. Bass, J. Cryst. Growth **47**, 613 (1979).
[2] C. E. C. Wood, G. M. Metze, J. D. Berry, and L. F. Eastman, J. Appl. Phys. **51**, 383 (1980).
[3] E. F. Schubert and K. Ploog, Jpn. J. Appl. Phys. (Lett.) **24**, L608 (1985); E. F. Schubert, A. Fischer, and K. Ploog, IEEE Trans. Electron Devices **ED-33**, 625 (1986).
[4] E. F. Schubert, J. B. Stark, B. Ullrich, and J. E. Cunningham, Appl. Phys. Lett. **52**, 1508 (1988); E. F. Schubert, J. B. Stark, T. H. Chin, and B. Tell, Appl. Phys. Lett. **53**, 293 (1988).
[5] M. Ilegems, J. Appl. Phys. **48**, 1278 (1977); W. V. McLevige, K. V. Vaidyanathan, B. G. Streetman, M. Ilegems, J. Comas, and L. Plew, Appl. Phys. Lett. **33**, 127 (1978); H. C. Casey, in *Atomic Diffusion in Semiconductors*, edited by D. Shaw (Plenum, London, 1973), p. 351.
[6] E. F. Schubert, J. M. Kuo, R. F. Kopf, H. S. Luftman, and L. C. Hopkins, unpublished (1989).
[7] E. F. Schubert, A. Fischer, and K. Ploog, IEEE Trans. Electron Devices **ED-33**, 625 (1986).
[8] E. F. Schubert, J. E. Cunningham, and W. T. Tsang, Solid State Commun. **63**, 591 (1987).
[9] G. Gillman, B. Vinter, E. Barbier, and A. Tardella, Appl. Phys. Lett. **52**, 972 (1988).
[10] It was pointed out that impurity-pair diffusion via vacancies is energetically favorable, since the charge state is conserved during the diffusion process. See M. E. Greiner and J. F. Gibbons, Appl. Phys. Lett. **44**, 750 (1984).
[11] R. A. Hamm, M. B. Panish, R. N. Nottenburg, Y. K. Chen, and D. A. Humphrey, Appl. Phys. Lett. **54**, 2586 (1989).
[12] E. F. Schubert, C. W. Tu, R. F. Kopf, J. M. Kuo, and L. M. Lunardi, Appl. Phys. Lett. **54**, 2592 (1989).
[13] W. Shockley, Solid-State Electron. **2**, 35 (1961).
[14] R. L. Headrick, L. C. Feldman, and I. K. Robinson, Appl. Phys. Lett. **55**, 442 (1989).
[15] A. F. J. Levi, S. L. McCall, and P. M. Platzman, Appl. Phys. Lett. **54**, 940 (1989).

Downloaded 25 Jun 2003 to 128.113.111.105. Redistribution subject to AIP license or copyright, see http://ojps.aip.org/japo/japcr.jsp